Nanoscale Research Letters

NANO EXPRESS Open Access

Investigation of Energy Band at Atomic-Layer-Deposited ZnO/β-Ga_2O_3 ($\bar{2}01$) Heterojunctions

Shun-Ming Sun, Wen-Jun Liu*, Yi-Fan Xiao, Ya-Wei Huan, Hao Liu, Shi-Jin Ding* and David Wei Zhang

Abstract

The energy band alignment of ZnO/β-Ga_2O_3 ($\bar{2}01$) heterojunction was characterized by X-ray photoelectron spectroscopy (XPS). The ZnO films were grown by using atomic layer deposition at various temperatures. A type-I band alignment was identified for all the ZnO/β-Ga_2O_3 heterojunctions. The conduction (valence) band offset varied from 1.26 (0.20) eV to 1.47 (0.01) eV with the growth temperature increasing from 150 to 250 °C. The increased conduction band offset with temperature is mainly contributed by Zn interstitials in ZnO film. In the meanwhile, the acceptor-type complex defect V_{Zn} + OH could account for the reduced valence band offset. These findings will facilitate the design and physical analysis of ZnO/β-Ga_2O_3 relevant electronic devices.

Keywords: β-Ga_2O_3, Contacts, ZnO, ALD

Introduction

Gallium oxide (Ga_2O_3) has been widely investigated as a promising ultrawide bandgap semiconductor material for next generation power electronic devices due to its unique properties [1]. Among various polymorphs (α, β, γ, δ, and ε), monoclinic β-Ga_2O_3 has the most thermal stability [2]. In addition, β-Ga_2O_3 has a room temperature bandgap of 4.5~4.9 eV, and excellent chemical stability [3]. Especially, β-Ga_2O_3 has a high bulk electron mobility of ~100 cm^2/V·s, much higher breakdown field of 8 MV/cm than that of SiC (3.18 MV/cm) or GaN (3 MV/cm) [4], and the carrier concentration can be easily modulated by doping Sn and Si [5, 6]. Therefore, β-Ga_2O_3-based devices including solar-blind photodetectors [7] and metal-oxide-semiconductor field-effect transistors (MOSFETs) [8] have been reported. However, limitations still exist in β-Ga_2O_3-based devices, such as the poor ohmic contact between the metal and β-Ga_2O_3 [9]. In recent year, inserting a high electron concentration metal-oxide-semiconductor interlayer, i.e., intermediate semiconductor layer (ISL) between the metal and Ga_2O_3, has been shown to be an effective resolution because the modulation of energy barrier at the interface [10–12].

Zinc oxide (ZnO) has attracted much attention because it has a large exciton binding energy of 60 meV, a high electron concentration of $>10^{19}$ cm^{-3}, and a strong cohesive energy of 1.89 eV. [13, 14] Additionally, the lattice mismatch between ZnO and Ga_2O_3 is within 5% [15]. Various deposition techniques have been developed to prepare ZnO film, including hydrothermal method [16, 17] and chemical vapor deposition (CVD). [18] However, hydrothermal method need a complicated process and the grow rate is quiet slow, and CVD generally requires quiet high growth temperature above 900 °C. These drawbacks make it challenging to be applied in devices. Recently, atomic layer deposition (ALD) has emerged as a promising technique, which exhibits excellent step coverage, atomic scale thickness controllability, good uniformity, and a relatively low deposition temperature. Consequently, atomic-layer-deposited ZnO on wide-bandgap semiconductors can reduce interface disorder and yield more controllable sample to examine the energy band alignment, which plays an important role in the carrier transport process [19]. Up to now, band alignment between Ga_2O_3 and atomic-layer-deposited ZnO has not been studied by experiment, although there are some reports about the

* Correspondence: wjliu@fudan.edu.cn; sjding@fudan.edu.cn
State Key Laboratory of ASIC and System, School of Microelectronics, Fudan University, Shanghai 200433, China

theoretical band alignment of ZnO and Ga_2O_3. [20] Therefore, understanding the energy band alignment of atomic-layer-deposited ZnO/β-Ga_2O_3 heterojunction is highly desirable for the design and physical analysis of relevant devices in the future. In this work, the energy band alignment of atomic-layer-deposited ZnO on β-Ga_2O_3 was characterized by X-ray photoelectron spectroscopy (XPS). Moreover, the influence of growth temperature of ZnO on the band alignment was also addressed.

Methods

β-Ga_2O_3 ($\bar{2}01$) substrates with a Sn doping concentration of ~ $3 \times 10^{18}/cm^3$ were diced into small pieces with the size of 6×6 mm^2. The diced samples were alternately cleaned in acetone, isopropanol by ultrasonic cleaning for each 10 min, subsequently rinsed with deionized water to remove residual organic solvents. After that, Ga_2O_3 substrates were transferred into an ALD reactor (Wuxi MNT Micro Nanotech co., LTD, China). The growth rate of ZnO films was ~ 1.6 Å/cycle. Both 40 and 5 nm ZnO films were grown on cleaned β-Ga_2O_3 using Zn $(C_2H_5)_2$ (DEZ) and H_2O at each temperature of 150, 200, and 250 °C, respectively. The thickness of prepared ZnO films was measured by Ellipsometer (Sopra GES-5E). The ZnO(40 nm)/β-Ga_2O_3 was used as bulk standard, and the ZnO(5 nm)/β-Ga_2O_3 was used to determine the band alignment, in the meanwhile the bare bulk β-Ga_2O_3 was used as the control sample. XPS (AXIS Ultra DLD, Shimadzu) measurements with a step of 0.05 eV were performed to measure the valence band maximum (VBM), Ga 2p and Zn 2p spectra. To avoid interference of surface oxidation and contamination, all samples were etched by Ar ion for 3 min with a voltage of 2 kV before XPS measurement. Note that all the XPS spectra were calibrated by C 1s peak at 284.8 eV for compensating the charging effect. To identify the bandgap, the optical transmittance spectra of Ga_2O_3 and ZnO were measured by ultraviolet-visible (UV-VIS) spectroscopy (Lambda 750, PerkinElmer, USA).

Results and Discussion

Figure 1 shows the variation of $(\alpha h\nu)^{1/n}$ as a function of photon energy for bulk β-Ga_2O_3 and the as-grown ZnO film deposited at 200 °C. The optical band gap (E_g) of the ZnO film and β-Ga_2O_3 can be determined by the Tauc's relation [21]: $(\alpha h\nu)^{1/n} = A(h\nu - E_g)$, where α is the absorption coefficient, A is a constant, $h\nu$ is the incident photon energy, E_g is the optical energy bandgap, n is 1/2 for the direct bandgap, and 2 for the indirect bandgap. Here, both ZnO and β-Ga_2O_3 have typical direct band gap that make the value of n is 1/2. Subsequently, E_g can be extracted by extrapolating the straight line portion to the energy bias at α = 0. Therefore, the extracted E_g of

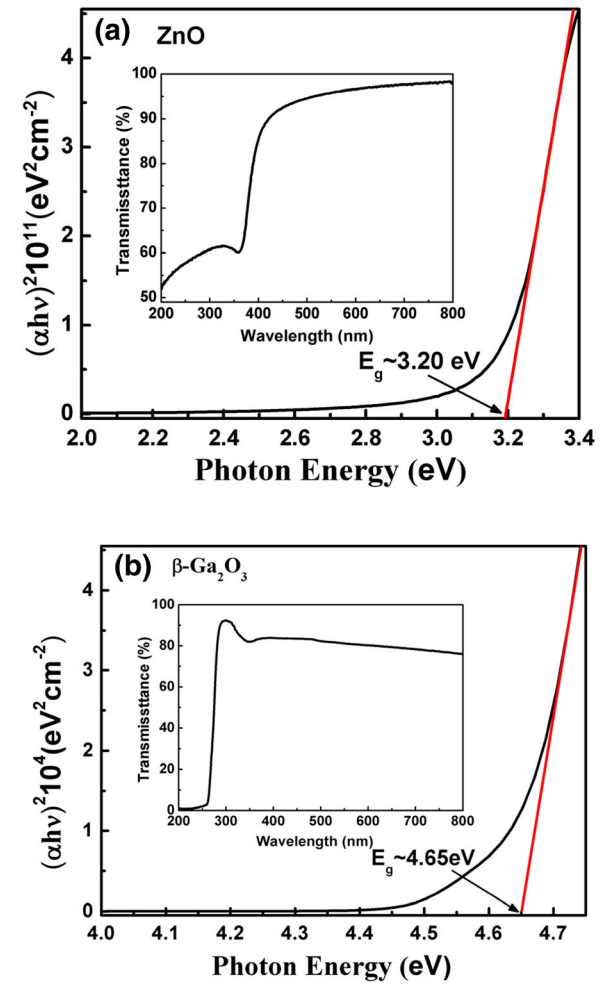

Fig. 1 The plot of $(\alpha h\nu)^2$ versus $h\nu$ for **a** ZnO film grown on quartz glass **b** β-Ga_2O_3 substrate. The inset shows the optical transmission spectra of ZnO and β-Ga_2O_3, respectively

ZnO and β-Ga_2O_3 are 3.20 eV and 4.65 eV, respectively, in good agreement with the reported. [22, 23]

The valence band offset (VBO) can be determined by Kraut's method using the following formula [24]

$$\Delta E_V = \left(E_{Ga\ 2p}^{Ga_2O_3} - E_{VBM}^{Ga_2O_3}\right) - \left(E_{Zn\ 2p}^{ZnO} - E_{VBM}^{ZnO}\right) - \left(E_{Ga\ 2p}^{Ga_2O_3} - E_{Zn\ 2p}^{ZnO}\right), \quad (1)$$

where $E_{Ga\ 2p}^{Ga_2O_3} - E_{VBM}^{Ga_2O_3}$ ($E_{Zn\ 2p}^{ZnO} - E_{VBM}^{ZnO}$) represents to the energy difference between Ga 2p (Zn 2p) core level (CL) and VBM of bulk β-Ga_2O_3 (ZnO), and $E_{Ga\ 2p}^{Ga_2O_3} - E_{Zn\ 2p}^{ZnO}$ denotes as the energy difference between Ga 2p and Zn 2p core levels. Figure 2 shows all CL spectra including Zn 2p of ZnO (40 nm)/β-Ga_2O_3 and ZnO (5 nm)/β-Ga_2O_3, Ga 2p of bulk Ga_2O_3 and ZnO (5 nm)/β-Ga_2O_3, as well as valence band spectra from bulk Ga_2O_3 and ZnO (40 nm)/β-Ga_2O_3. Figure 2a presents the CL spectra of

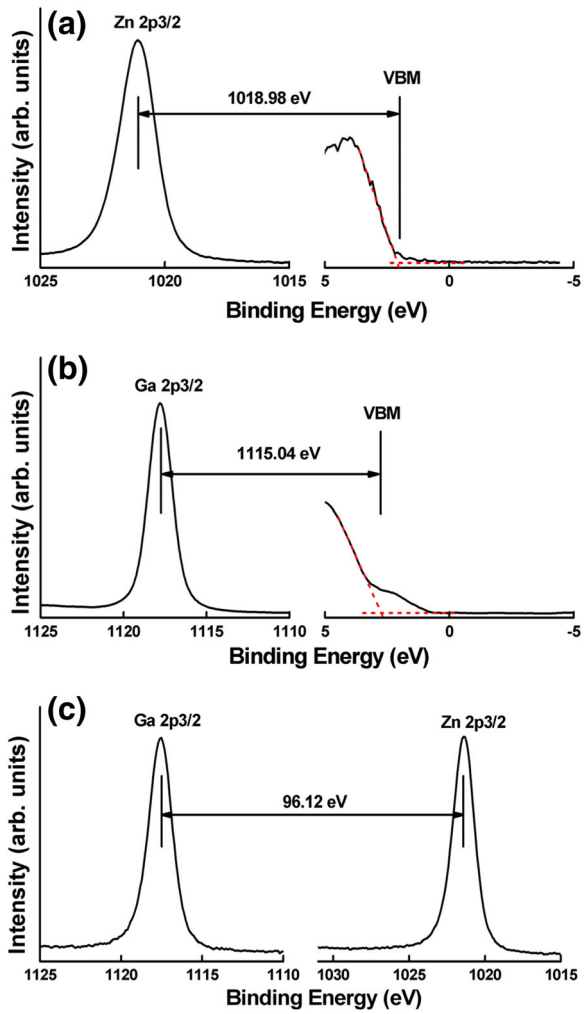

Fig. 2 High-resolution XPS spectra for core level and valence band maximum(VBM) of **a** Zn 2p core level spectrum and VBM from 40 nm ZnO/β-Ga_2O_3, **b** Ga 2p core level spectrum and VBM from bare β-Ga_2O_3, and **c** the core level spectra of Ga 2p and Zn 2p obtained from high-resolution XPS spectra of 5 nm ZnO/β-Ga_2O_3

Zn 2p on the ZnO (40 nm)/β-Ga_2O_3, which is quiet symmetrical indicating the uniform bonding state, and the peak locates at 1021.09 eV corresponds the Zn-O bond [25]. The VBM can be determined using a linear extrapolation method [26]. The VBM of ZnO is located at 2.11 eV. In Fig. 2b, the peak located at 1117.78 eV corresponds to the Ga-O bond [27] and the VBM of Ga_2O_3 is deduced to be 2.74 eV according to the method mentioned above. The CLs of Zn 2p and Ga 2p in the ZnO (5 nm)/β-Ga_2O_3 are shown in Fig. 2c. According to Eq. (1), the VBO at the interface of ZnO/Ga_2O_3 is determined to be 0.06 eV.

Based on the calculated E_g and ΔE_V, the conduction band offset (CBO) at the ZnO/Ga_2O_3 interface can be easily deduced from the following equation:

$$\Delta E_C = E_g^{Ga_2O_3} - E_g^{ZnO} - \Delta E_V, \quad (2)$$

where $E_g^{Ga_2O_3}$ and E_g^{ZnO} are the energy bandgap for β-Ga_2O_3 and ZnO, respectively. The detailed energy band diagram for ZnO/β-Ga_2O_3 is depicted in Fig. 3. The interface has a type-I band alignment, where both conduction and valence band edges of ZnO are located within the bandgap of β-Ga_2O_3.

To further examine the effect of the growth temperature on the band alignment between ZnO and β-Ga_2O_3, the ZnO films are also grown at 150 and 250 °C. Note that ZnO films prepared by ALD at the temperatures of 150–250 °C have poly-crystalline nature. Figure 4 shows the high-resolution O 1s XPS spectra of the ZnO films grown at different temperatures. Each O 1s spectrum can be well separated into three components using Gaussian-Lorentzian function. The peaks centered at 530.0 (O1), 531.6 (O2), and 532.4 (O3) eV correspond to the Zn-O bands, oxygen vacancies, and –OH group [28, 29], respectively. The relative percentage of different components is also calculated according to the peak area, digested in Fig. 4. It shows that the relative content of oxygen vacancies increases from 10.7 to 15.0% due to the decomposition of precursors and the increase of Zn interstitials. However, the –OH counterpart reduces from 5.1 to 1.9% because of more complete reactions between DEZ precursors and surface –OH groups in this temperature range [30].

Figure 5 shows the band offsets of ZnO/β-Ga_2O_3 heterojunctions as a function of growth temperature. The CBO increases from 1.26 to 1.47 eV with the growth temperature varying from 150 to 250 °C. The native donor defects include the Zn anti-position, oxygen vacancies, and Zn interstitials. However, the formation energy of anti-position atoms is so high that its concentration is extremely low. The Zn interstitials have more influence on the conduction band minimum (CBM) than that of the oxygen vacancy because the CBM is mainly dominated by the 4s orbit of Zn atom. [31] As a result, the increased CBO of 0.21 eV could be mainly contributed by Zn interstitials. On the other hand, the VBO reduces from 0.20 to 0.01 eV with the growth temperature increasing from 150 to 250 °C. The native acceptor defects include the O anti-position, Zn vacancies, and oxygen interstitials [32], whose formation energies are high and their number can be even negligible. Furthermore, the most native acceptor levels are deep within the ZnO bandgap, thus they have little effect on the VBM [33]. However, $V_{zn} + OH$ is favorable to be presented duo to the low formation

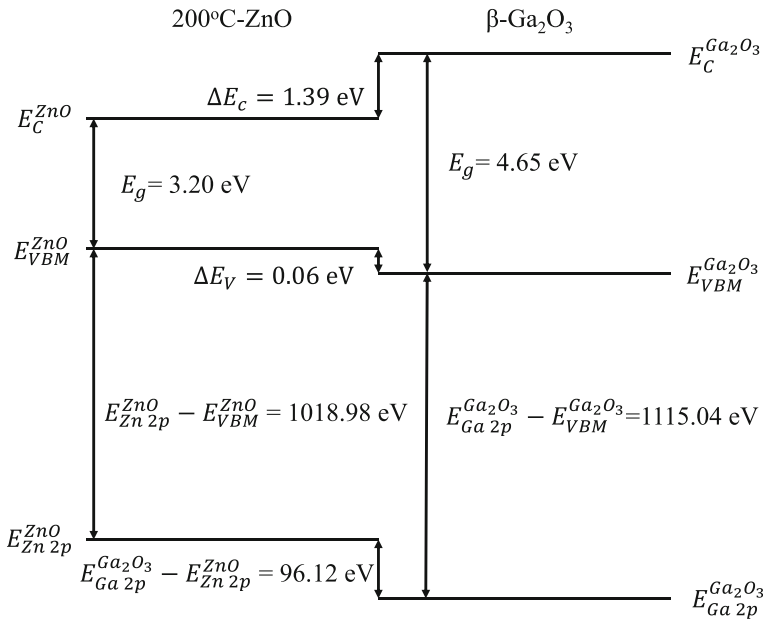

Fig. 3 Schematic band alignment diagram of the ZnO (200 °C)/β-Ga_2O_3 heterojunction

energy, [34] V_{zn} + OH may occur with an electron belonging to OH bonds. The lattice hydrogen H^+ ion acts as a compensating center, and it can bind with the V_{Zn} around the dislocation and stacking faults core, ensuring the acceptor-type complex defect for p-type conductivity [35]. More residual –OH groups in the ZnO film are obtained at a lower growth temperature, i.e., 150 °C [36]. The acceptor level near the VBM reduces with the temperature, leading to an effectively downward shift in E_V of ZnO, thus the ΔE_V becomes lower. Therefore, the ZnO deposited at lower temperature could be more efficiently to reduce the barrier height at the interface between the metal and Ga_2O_3.

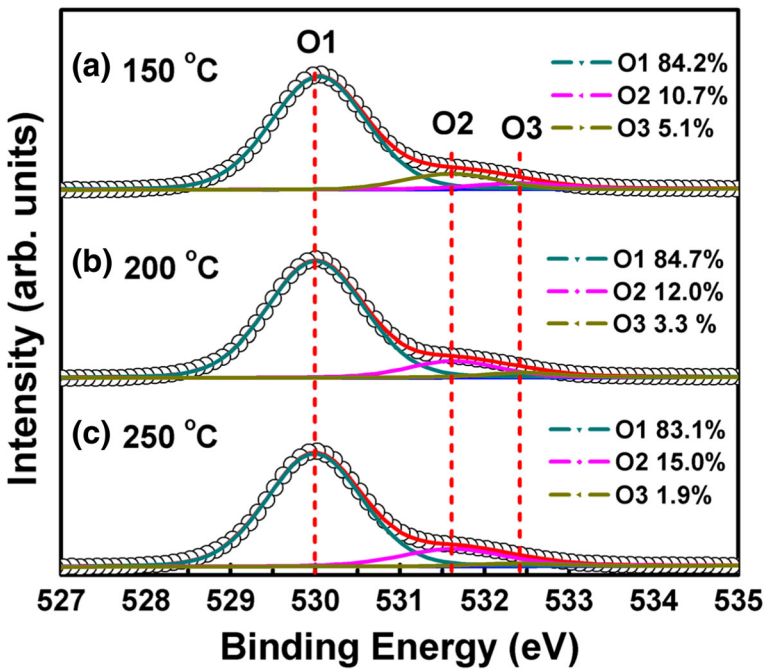

Fig. 4 High-resolution O 1 s XPS spectra of the ZnO films grown at **a** 150 °C, **b** 200 °C, and **c** 250 °C, respectively

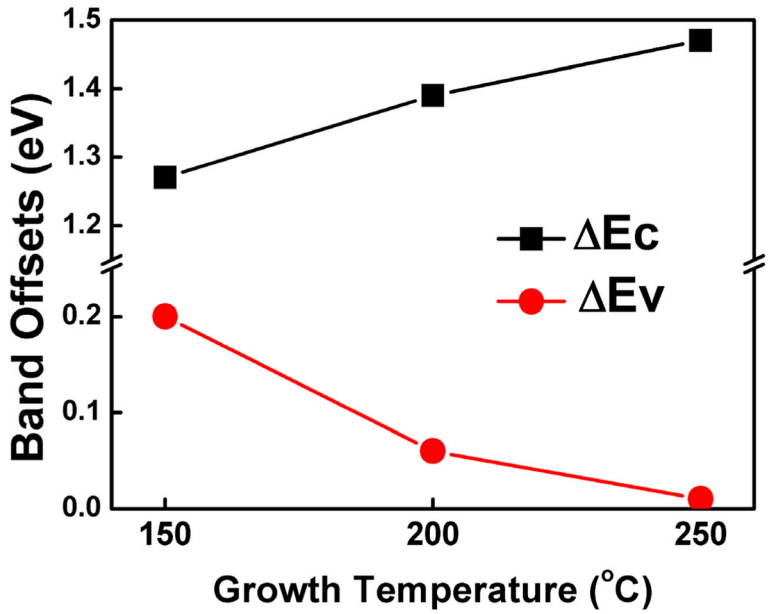

Fig. 5 The conduction and valence band offsets of atomic-layer-deposited ZnO/β-Ga_2O_3 heterojunctions fabricated at different temperatures

Conclusions

In summary, the energy band alignment at atomic-layer-deposited ZnO/β-Ga_2O_3 ($\bar{2}01$) was characterized by XPS. A type-I band alignment formed at the ZnO/β-Ga_2O_3 interface. The conduction band offset increased from 1.26 to 1.47 eV while the valence band offset decreased from 0.20 to 0.01 eV with the temperature increasing from 150 to 250 °C. These observations suggest that the ZnO deposited at lower temperature is favorable to be a promising ISL to reduce the electron barrier height at the ZnO/β-Ga_2O_3 interface.

Abbreviations

ALD: Atomic layer deposition; CBM: Conduction band minimum; CBO: Conduction band offset.; CVD: Chemical vapor deposition; DEZ: Zn$(C_2H_5)_2$; Ga_2O_3: Gallium oxide; GaN: Gallium nitride; ISL: Intermediate semiconductor layer; MOSFETs: Metal-oxide-semiconductor field-effect transistors; OH: Hydroxyl; SiC: Silicon carbide; UV-VIS: Ultraviolet-visible spectroscopy; VBM: Valence band maximum; VBO: Valence band offset; XPS: X-ray spectroscopy; ZnO: Zinc oxide

Funding

The authors would like to acknowledge the financial support in part by the National Natural Science Foundation of China (Nos. 61474027, and 61774041), in part by the National Key Technologies Research and Development Program of China (Nos. 2015ZX02102-003, and 2017YFB0405600).

Availability of Data and Materials

The datasets supporting the conclusions of this manuscript are included within the manuscript.

Authors' Contributions

SMS, YFX, YWH, and HL conducted the extensive experiments and analyzed the data. WJL and SJD supervised the project and wrote the manuscript. DWZ helped to review and discuss the manuscript. All authors read and approved the final manuscript.

Competing Interests

The authors declare that they have no competing interests.

Publisher's Note

Received: 2 November 2018 Accepted: 9 December 2018
Published online: 24 December 2018

References

1. Rafique S, Han L, Zhao H (2017) Ultrawide bandgap β-Ga_2O_3 thin films: growths, properties and devices. ECS Trans 80(7):203–216
2. Si M, Yang L, Zhou H, Ye PD (2017) β-Ga2O3 nanomembrane negative capacitance field-effect transistors with steep subthreshold slope for wide band gap logic applications. ACS Omege 2:7136–7140
3. Mastro MA, Kuramata A, Calkins J, Kim J, Ren F, Peartong SJ (2017) Opportunities and future directions for Ga_2O_3. ECS J Solid State Sc 6(5): 356–359
4. Green AJ, Chabak KD, Heller ER, Fitch RC, Baldini M, Fiedler A, Irmscher K, Wagner G, Galazka Z, Tetlak SE, Crespo A, Leedy K, Jessen GH (2016) 3.8-MV/cm breakdown strength of MOVPE-grown Sn-doped β-Ga_2O_3 MOSFETs. IEEE Electron Device Lett 37(7):902–905
5. Moser NA, McCandless JP, Crespo A, Leedy KD, Green AJ, Heller ER, Chabak KD, Peixoto N, Jessen GH (2017) High pulsed current density β-Ga_2O_3 MOSFETs verified by an analytical model corrected for interface charge. Appl Phys Lett 110:143505
6. Baldini M, Albrecht M, Fiedler A, Irmscher K, Klimm D, Schewski R, Wagner G (2016) Semiconducting Sn-doped β-Ga_2O_3 homoepitaxial layers grown by metal organic vapour-phase epitaxy. J Mater Sci 51:3650–3656
7. Feng W, Wang X, Zhang J, Wang L, Zheng W, Hu PA, Cao W, Yang B (2014) Synthesis of two-dimensional β-Ga_2O_3 nanosheets for high-performance solar blind photodetectors. J Mater Chem C 2:3254–3259
8. Higashiwaki M, Sasaki K, Kamimura T, Wong MH, Krishnamurthy D, Kuramata A, Masui T, Yamakoshi S (2013) Depletion-mode Ga_2O_3 metal-oxide-semiconductor field-effect transistors on β-Ga_2O_3 (010) substrates and temperature dependence of their device characteristics. Appl Phys Lett 103:123511
9. Higashiwaki M, Sasaki K, Kuramata A, Masui T, Yamakoshi S (2012) Gallium oxide (Ga_2O_3) metal-semiconductor field-effect transistors on single-crystal β-Ga_2O_3 (010) substrates. Appl Phys Lett 100:013504

10. Carey PH, Yang J, Ren F, Hays DC, Pearton SJ, Jang S, Kuramata A, Kravchenko II (2017) Ohmic contacts on n-type β-Ga_2O_3 using AZO/Ti/au. AIP Adv 7:095313
11. Wu Z, Jiao L, Wang X, Guo D, Li W, Li L, Huang F, Tang W (2017) A self-powered deep-ultraviolet photodetector based on an epitaxial Ga_2O_3/Ga:ZnO heterojunction. J Mater Chem C 5:8688–8693
12. Huan YW, Sun SM, Gu CJ, Liu WJ, Ding SJ, Yu HY, Xia CT, Zhang DW (2018) Recent advances in β-Ga_2O_3-metal contacts. Nanoscale Res Lett 13:246
13. Hong SK, Hanada T, Makino H, Chen Y, Ko HJ, Yao T (2001) Band alignment at a ZnO/GaN (0001) heterointerface. Appl Phys Lett 78:3349
14. Shi K, Zhang PF, Wei HY, Jiao CM, Li CM, Liu XL, Yang SY, Zhu QS, Wang ZG (2012) Energy band alignment of MgO (111)/ZnO (0002) heterojunction determined by X-ray photoelectron spectroscopy. Solid State Commun 152:938–940
15. Zhao B, Wang F, Chen H, Zheng L, Su L, Zhao D, Fang X (2017) An ultrahigh responsivity (9.7 mA W^{-1}) self-powered solar-blind photodetector based on individual ZnO–Ga_2O_3 Heterostructures. Adv Funct Mater 27:1700264
16. Guo DY, Shi HZ, Qian YP, Lv M, Li PG, Su YL, Liu Q, Chen K, Wang SL, Cui C (2017) Fabrication of β-Ga_2O_3/ZnO heterojunction for solar-blind deep ultraviolet photodetection. Semicond Sci Technol 32:03LT01
17. Wei L, Liu QX, Zhu B, Liu WJ, Ding SJ, Lu HL, Jiang A, Zhang DW (2016) Low-cost and high-productivity three-dimensional nanocapacitors based on stand-up ZnO nanowires for energy storage. Nanoscale Res Lett 11:213
18. Ohnishi S, Hirokawa Y, Shiosaki T, Kawabata A (1978) As-grown CVD ZnO optical waveguides on sapphire. Appl Phys Lett 33(5):406–407
19. Shen K, Wu K, Wang D (2013) Band alignment of ultra-thin hetero-structure ZnO/TiO_2 junction. Mater Res Bull 51:141–144
20. Chen M, Zhao B, Hu G, Fang X, Wang H, Wang L, Luo J, Han X, Wang X, Pan C, Wang ZL (2018) Piezo-phototronic effect modulated deep UV photodetector based on ZnO-Ga_2O_3 Heterojuction microwire. Adv Funct Mater 28:1706379
21. Eom K, Lee D, Kim S, Seo H (2018) Modified band alignment effect in ZnO/Cu_2O heterojunction solar cells via Cs_2O buffer insertion. J Phys D Appl Phys 51(5):055101
22. Jia Y, Zeng K, Wallace JS, Gardella JA, Singisetti U (2015) Spectroscopic and electrical calculation of band alignment between atomic layer deposited SiO_2 and β-Ga_2O_3 ($\bar{2}$01). Appl Phys Lett 106:102107
23. Dewan S, Tomar M, Goyal A, Kapoor AK, Tandon RP, Gupta V (2016) Study of energy band discontinuity in NiZnO/ZnO heterostructure using X-ray photoelectron spectroscopy. Appl Phys Lett 108:211603
24. Kraut EA, Grant RW, Waldrop JR, Kowalczyk SP (1980) Precise determination of the valence-band edge in X-ray photoemission spectra: application to measurement of semiconductor interface potentials. Phys Rev Lett 44(24):1620–1623
25. You JB, Zhang XW, Song HP, Ying J, Guo Y, Yang AL, Yin ZG, Chen NF, Zhu QS (2009) Energy band alignment of interface determined by x-ray photoelectron spectroscopy. J Appl Phys 106:043709
26. Carey PH, Ren F, Hays DC, Gila BP, Pearton SJ, Jang S, Kuramata A (2017) Valence and conduction band offsets in AZO/Ga_2O_3 heterostructures. Vacuum 141:103–108
27. Carey PH, Ren F, Hays DC, Gila BP, Pearton SJ, Jang S, Kuramata A (2017) Band alignment of atomic layer deposited SiO_2 and $HfSiO_4$ with ($\bar{2}$01) β-Ga_2O_3. Jpn J Appl Phys 56:071101
28. Major S, Kumar S, Bhatnagar M, Chopra KL (1986) Effect of hydrogen plasma treatment on transparent conducting oxides. Appl Phys Lett 49(7):394–396
29. Wang ZG, Zu XT, Zhu S, Wang LM (2006) Green luminescence originates from surface defects in ZnO nanoparticles. Phys E 35(1):199–202
30. Saha D, Das AK, Ajimsha RS, Misra P, Kukreja LM (2013) Effect of disorder on carrier transport in ZnO thin films grown by atomic layer deposition at different temperatures. J Appl Phys 114:043703
31. Kobayashi A, Sankey OF, Volz SM, Dow JD (1983) Semiempirical tight-binding band structures of wurtzite semiconductors: AlN, CdS, CdSe, ZnS, and ZnO. Phys Rev B 28(2):935–945
32. Heiland G, Mollwo E, Stockmann Z (1959) Electronic processes in zinc oxide. Solid State Phys 8:191–323
33. Vidya R, Ravindran P, Fjellvag H, Svensson BG, Monakhov E, Ganchenkova M, Nieminen RM (2011) Energetics of intrinsic defects and their complexes in ZnO investigated by density functional calculations. Phys Rev B 83(4):2385
34. Xue X, Liu L, Wang Z, Wu Y (2014) Room-temperature ferromagnetism in hydrogenated ZnO nanoparticles. J Appl Phys 115(3):1019
35. Senthilkumar K, Yoshida T, Fujita Y (2018) Formation of D–V Zn complex defects and possible p-type conductivity of ZnO nanoparticle via hydrogen adsorption. J Mater Sci 53(17):11977–11985
36. Fang M, Qi L, Zhang C, Chen Q (2016) Effects of thickness and deposition temperature of ALD ZnO on the performance of inverted polymer solar cells. J Mater Sci Mater Electron 27:10252–10258